© 2018. Published by The Company of Biologists Ltd | Journal of Experimental Biology (2018) 221, jeb171199. doi:10.1242/jeb.171199

RESEARCH ARTICLE

Aerodynamic characteristics along the wing span of a dragonfly *Pantala flavescens*

Csaba Hefler, Huihe Qiu* and Wei Shyy

ABSTRACT

We investigated the characteristics of interwing aerodynamic interactions across the span of the high aspect ratio, flexible wings of dragonflies under tethered and free-flying conditions. This revealed that the effects of the interactions on the hindwings vary across four spanwise regions. (i) Close to the wing root, a trailing-edge vortex (TEV) is formed by each stroke, while the formation of a leading-edge vortex (LEV) is limited by the short translational distance of the hindwing and suppressed by the forewing-induced flow. (ii) In the region away from the wing root but not quite up to midspan, the formation of the hindwing LEV is influenced by that of the forewing LEV. This vortex synergy can increase the circulation of the hindwing LEV in the corresponding cross-section by 22% versus that of the hindwing in isolation. (iii) In the region about half-way between the wing root and wing tip there is a transition dominated by downwash from the forewing resulting in flow attached to the hindwing. (iv) A LEV is developed in the remaining, outer region of the wing at the end of a stroke when the hindwing captures the vortex shed by the forewing. The interaction effects depend not only on the wing phasing but also on the flapping offset and flight direction. The aerodynamics of the hindwings vary substantially from the wing root to the wing tip. For a given phasing, this spanwise variation in the aerodynamics can be exploited in the design of artificial wings to achieve greater agility and higher efficiency.

KEY WORDS: Flapping flight, Dragonfly, Interaction, Leading edge vortex, Aerodynamics

INTRODUCTION

Dragonflies are among the most agile flying insects (Shyy et al., 2008, 2013; Combes et al., 2012). Observations on free-flying dragonflies reveal that in-phase flapping generates high aerodynamic forces for quick, demanding maneuvers or takeoff, while out-of-phase flapping is favored for steady flight and hovering (Norberg, 1975; Alexander, 1984; Azuma and Watanabe, 1988; Rüppell, 1989; Wakeling and Ellington, 1997; Wang et al., 2003).

Numerical (Lan and Sun, 2001; Sun and Lan, 2004; Wang and Russell, 2007) and experimental (Maybury and Lehmann, 2004; Usherwood and Lehmann, 2008; Hu and Deng, 2014) studies of hovering flight using either horizontal or inclined strokes have shown the downwash effect to be detrimental to vertical force generation. Downwash attenuates hindwing leading-edge vortex (LEV) circulation (Maybury and Lehmann, 2004) in the case of forewing-led phasing. In the case of hindwing-led phasing, however, hovering with all four wings consumes 22% less power than hovering with just two wings (Usherwood and Lehmann, 2008).

One of the key attributes of a flapping wing in generating lift is the delayed stall by the LEV, which can result in a substantial aerodynamic force for a flapping wing system (Dickinson and Götz, 1993; Ellington et al., 1996; Dickinson et al., 1999). The LEV generates a low-pressure area, which results in an increased suction force on the wing surface (Sane, 2003; Birch et al., 2004; Shyy and Liu, 2007). Direct vortex interactions could advance or delay LEV formation and shedding and, at the same time, strengthen or attenuate LEV circulation.

Maybury and Lehmann (2004) and Rival et al. (2011) experimentally revealed that a trailing-edge vortex (TEV) shed by the forewing promotes the formation of the hindwing LEV in the case of 90 deg phasing of the wings. Hsieh et al. (2010) performed 2D numerical simulation and explained that the increase in hindwing thrust at 90 deg phasing is due to the fusion of the forewing downstroke TEV with the LEV of the upstroking hindwing. In a counter-stroking setup, however, a similar vortex fusion amplifies the lift generated by the downstroking hindwing (Hsieh et al., 2010). Furthermore, experimental (Hu and Deng, 2014) and numerical (Xie and Huang, 2015) studies showed that the forewing TEV and the hindwing LEV interact synergistically if they are formed in close proximity.

Additionally, Broering et al. (2012) concluded from their 2D numerical simulation of forward flight that at a system level, the tandem configuration when the wings are flapping in phase produces a large thrust at a high propulsive efficiency but at the cost of lift efficiency, while a 90 or 180 deg phase flapping cycle greatly reduces the power consumption at the expense of thrust production. Most recently, Zheng et al. (2015, 2016a,b) studied the underlying interaction features of pitching and plunging wings that are either flexible or rigid while hovering (Zheng et al., 2016b), and both while hovering and in forward flight (Zheng et al., 2015, 2016a) at critical time instants when large force modulation occurred as a result of aerodynamic interactions. They also found synergy between the forewing TEV and the hindwing LEV when the two wings were flapping in phase. When the wings were flapping out of phase, the TEV shed by the forewing could either enhance the hindwing LEV (when their spins were opposite) or attenuate it (when their spins were the same) upon reaching the hindwing. They also showed that in some cases the flow induced by the forewing LEV could increase the hindwing's effective angle of attack, resulting in an earlier LEV formation.

None of the studies mentioned above specifically addressed the variation in interaction features across the span of root-flapping tandem wings, which could be of major importance considering the high aspect ratio of dragonfly wings. Furthermore, all experimental and numerical models use rigid wing modeling or simplified geometries or they change selected parameters (like the wing

Department of Mechanical and Aerospace Engineering, The Hong Kong University of Science and Technology, Clear Water Bay, Kowloon, Hong Kong SAR, China.

*Author for correspondence (meqiu@ust.hk)

C.H., 0000-0003-3734-6470; H.Q., 0000-0002-2135-9771; W.S., 0000-0001-6670-5394

Received 4 October 2017; Accepted 4 August 2018

Journal of Experimental Biology (2018) 221, jeb171199. doi:10.1242/jeb.171199

List of symbols and abbreviations

C_{HW}	hindwing chord
FD	forewing LEV formed during the downstroke
FFT	fast Fourier transform
FU	forewing LEV formed during the upstroke
HD	hindwing LEV formed during the downstroke
HU	hindwing LEV formed during the upstroke
LEV	leading-edge vortex
min	lowest value of the correlation plane
P_1	peak height of the highest correlation peak
P_2	peak height of the second-highest correlation peak
Q	relative correlation peak value (Q= P_1–min/P_2–min)
rms	root mean square
S_{HW}	hindwing span
t	time
t^*	dimensionless time (t^*=t/T)
T	flapping period
TEV	trailing-edge vortex
TR-SPIV	time-resolved stereo particle image velocimetry
ϕ	wing positional angle
Γ	circulation

phasing) in isolation. In a recent numerical study, Hefler et al. (2017) assessed the implications of various interaction scenarios across the span of the wings of a free-flying dragonfly on vertical and horizontal force generation. More studies involving live specimens are needed to obtain a deeper understanding of dragonfly aerodynamics for aircraft design (Hedrick et al., 2015; Chin and Lentink, 2016).

A few groups have attempted full-span qualitative and quantitative studies involving live dragonflies (Somps and Luttges, 1985, 1986; Yates, 1986; Reavis and Luttges, 1988; Thomas et al., 2004; Bomphrey et al., 2016). Thomas et al. (2004) studied the aerodynamics of tethered and free-flying dragonflies qualitatively using smoke visualization in a wind tunnel whereas Bomphrey et al. (2016) did so using particle image velocimetry (PIV). The first group reported that the forewing LEV spans the dragonfly body from tip to tip, while the hindwing typically exhibits attached flow (Thomas et al., 2004). However, Lai and Shen (2012) hypothesized that the LEV extending over the body could be caused by the wind tunnel flow and the tilted body alignment of the dragonfly during takeoff (Lai and Shen, 2012).

The goal of the present study was to explore the spanwise variance in flow dynamics of a dragonfly in still air. Previous studies found that when the hindwing is leading the phasing by approximately 90 deg, the interaction between the forewing and the hindwing significantly affects only the hindwing, especially in the case of forward flight (Maybury and Lehmann, 2004; Hsieh et al., 2010; Rival et al., 2011; Broering et al., 2012; Hu and Deng, 2014; Xie and Huang, 2015; Zheng et al., 2016a). Therefore, we focused on how the presence of the forewing affects the hindwing.

MATERIALS AND METHODS

Live dragonfly specimens

The subject of this study was *Pantala flavescens* (Fabricius 1798), a very common dragonfly species found on all continents except Antarctica (Fig. 1A,B). It is a medium-sized dragonfly with a wingspan of 80–90 mm and a body length of about 50 mm. Specimens were caught near the Clear Water Bay campus of the Hong Kong University of Science and Technology. Experiments were performed with the dragonflies a few hours after capture so that they could adapt to the lower temperature (19°C) in the laboratory. The specimens that were vigorous and showed greater consistency in their flapping were selected for the experiments. For the sake of repeatability and to ensure that the measurement cross-section was set precisely, we measured the flow features of tethered specimens. Flow measurements of free-flying dragonflies were also taken for comparison. Altogether, seven specimens were measured in tethered flight and another seven in free flight.

Experimental procedures for flow measurements in tethered flight

We measured the flow around the flapping wings of tethered specimens according to the following procedures (Fig. 1C). The dragonfly thorax was glued to a transparent glass plate using epoxy glue. Great care was taken to minimize any restriction on the motion of the wings and the abdomen. The dragonfly was glued to the glass plate in such a way that its head was below the horizontal axis while its abdomen was above to provide an optimal viewing angle for the two cameras when the wings were in motion. This is not the natural posture of a forward flying dragonfly, and it is possible that the specimen might use slightly altered wing strokes. Nevertheless, the experiments were unlikely to be affected as they were conducted in a black-walled chamber using a bright laser light, which made it impossible for the dragonfly to find any reference points for visual identification of its environment. The 1.1 mm thick glass with a reducing width toward the dragonfly abdomen was rigid enough to eliminate vibrations and its transparency ensured minimal glare. The glass plate was held by a precision stage, allowing the specimen to be moved sideways. The flow fields were measured by time-resolved stereo particle image velocimetry (TR-SPIV, LaVision GmbH) across the span of the wing. The dragonfly was stimulated with a thin carbon fiber rod. To minimize disturbances to the flow caused by the rod, the specimen was first allowed to grab the rod akin to perching on a tree branch. The rod was then pulled away, causing the dragonfly to instinctively start flapping. The tethered dragonfly flapped for 10 s or more, and our particle image velocimetry (PIV) setup could record 2 s of it with the set recording frequency. This set of procedures applied to experiments involving both dragonflies with all four wings intact and dragonflies with one of their forewings removed.

In the tandem-wing experiment, the cross-sectional flow measurement started 3 mm from the wing root with a spacing of 5 mm (Fig. 1B), which is about 12% of the span of the entire hindwing (S_{HW}). The measurement cross-sections have an uncertainty of ±0.5 mm (±1.2% of S_{HW}). We divided the wings of the tethered dragonfly into seven equidistant measurement cross-sections (Fig. 1B). A non-dimensional time t^* was defined, normalized by the period T of flapping, in order for us to present selected frames from the flapping cycle, where t^*=t/T=0 and t=0 denotes the moment when the hindwing starts its downstroke motion.

To assess the effect of interwing interaction on the hindwing aerodynamics, tethered dragonflies were also measured with and without one of their forewings removed. The results in Table 1 show that the hindwing kinematics changed little after removal of the forewing. In cases where one of the forewings was removed, the measurement spacing of 5 mm was retained but the number of measurement cross-sections was reduced to avoid exhausting the specimen too much.

Experimental procedures for flow measurements in free flight

In order to measure free-flight flow dynamics, a still air chamber of 2 cubic meters was built indoors (Fig. 1D). Black curtains were

Journal of Experimental Biology (2018) 221, jeb171199. doi:10.1242/jeb.171199

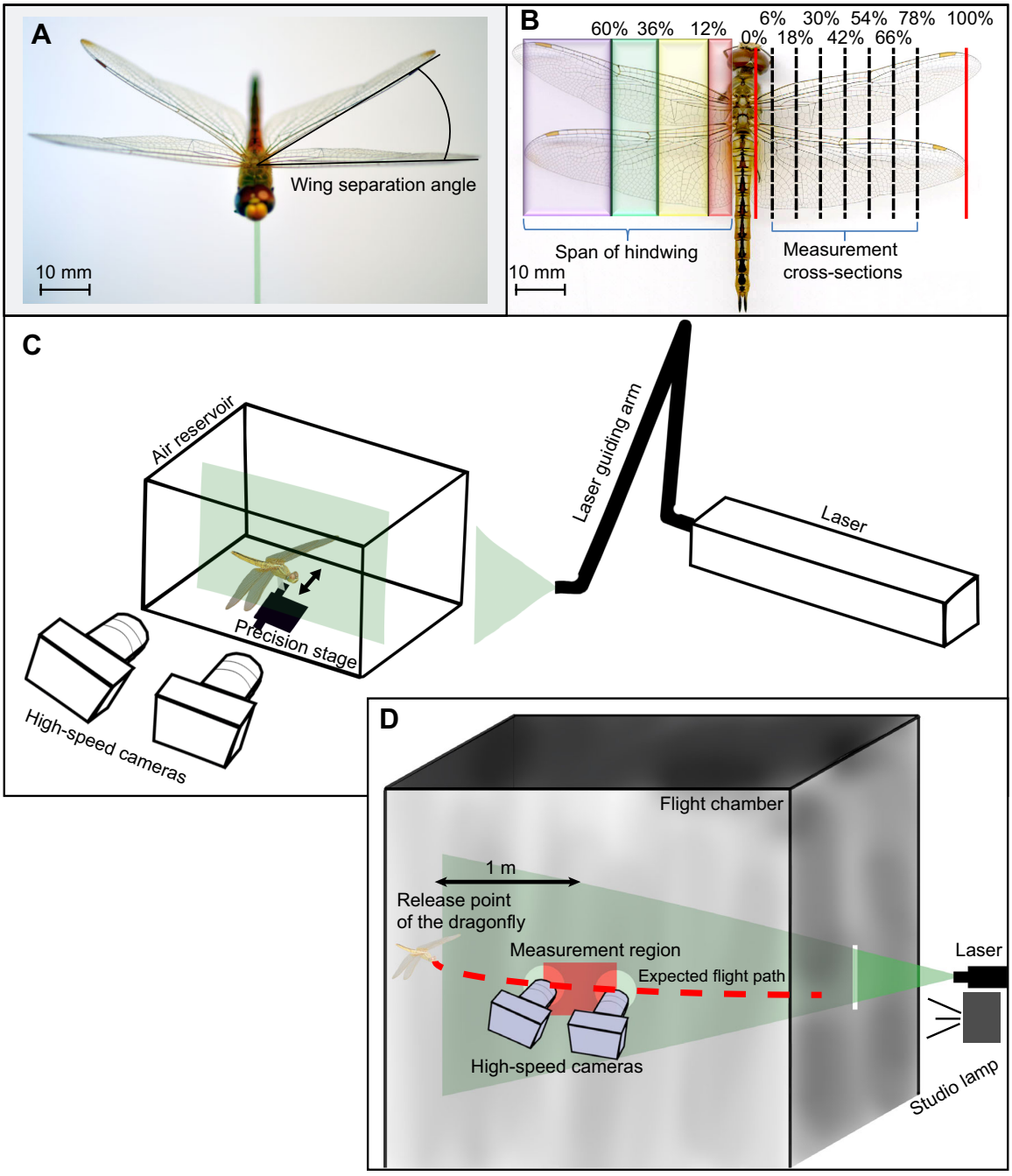

Fig. 1. Experimental procedure. (A) The tethered dragonfly and the definition of the wing separation angle. (B) Measurement of cross-sections, the definition of the hindwing span (S_{HW}), and the root (red), inner (yellow), transition (green) and outer (purple) regions. (C) Setup for the tethered measurement. (D) Setup for the free-flight measurement.

hung in the chamber but openings were made into the walls for the high-speed cameras, the laser light and the guiding light. There was no air flow inside the chamber throughout the experiments. The dragonflies were held in a horizontal position by hand and then carefully released inside the flight chamber at about 1 m from the measurement field of view. By visually observing the recorded flight, we ascertained that the specimens were able to fly forward naturally in the cases evaluated. In our measurements, we only processed the PIV images after the dragonfly had been making a quasi-steady-state forward flight. The transient period right after releasing the dragonfly into the chamber was not considered. A strong incandescent studio lamp was used as the guiding light. By placing the guiding light next to the laser light sheet of the PIV system, we could guide the dragonflies to fly nearly parallel to the light sheet. The flight duration of the free-flying experiments was 2–3 s, long before the specimen reached the other end of the flight chamber.

Setup and settings of the PIV system for flow measurements

To measure the flow field around the flapping wings with TR-SPIV, flow field areas of approximately 130×70 mm (tethered and free flight) and 90×55 mm (tethered with one forewing removed) were recorded using two high-speed CMOS sensor cameras (VC-Phantom M310). The cameras were equipped with macro lenses

Journal of Experimental Biology (2018) 221, jeb171199. doi:10.1242/jeb.171199

Table 1. Mean kinematic parameters of the dragonfly specimens (seven specimens in tethered flight and seven specimens in free flight)

Specimen	Flapping frequency (Hz)	Phase difference (deg)	Stroke-plane angle relative to the body (deg)	Forewing ϕ amplitude (deg)	Hindwing ϕ amplitude (deg)	Baseline of forewing ϕ (deg)	Baseline of hindwing ϕ (deg)
Tethered	24.4±1.2	82±14.9	64±2.2	65±3.4	65±3.5	6.8±5.5	0
Tethered with one forewing removed	24.8±2	–	64±2.5	–	63±5	–	1.25
Free flight	36.3±5.3	92±9.9	64±4.1	Indeterminate	Indeterminate	Indeterminate	Indeterminate

Data are means±s.d. for seven specimens in tethered flight and seven specimens in free flight. ϕ, wing positional angle.

mounted on Scheimpflug adapters. The closed air reservoir was seeded with a mist of olive oil from a compressed air aerosol generator (LaVision GmbH). The seeding particles were of a submicrometer diameter. Before each measurement, the reservoir was allowed time to calm after the seeding pump had induced a flow. The oil mist was illuminated by a 20 mJ laser (VL-Nd: YLF, 527 nm, Photonics Industries) producing double pulses at 1000 Hz. The interval of the double pulse, which varied from 150 to 200 µs, was determined by the estimated velocity range of the flow around the flapping wings. The laser beam was delivered by a compact light guiding arm (LaVision GmbH) coupled with light-sheet optics, which provided a laser sheet approximately 2 mm thick. The laser and the PIV cameras were controlled using the DaVis version 8.2.1 software package and were triggered by a common high-speed controller. The PIV cameras were calibrated with the built-in calibration routine in DaVis using a 310×310 mm dual plane calibration plate (LaVision, type 309-15). The calibration was then refined using a built-in auto-calibration algorithm in two steps. The recorded PIV data were processed also using DaVis. The particle images were preprocessed by local intensity normalization. Vector fields were computed in stereo cross-correlation mode, starting with interrogation windows of 96×96 pixels, reducing stepwise to 32×32 pixels for the final pass. With an overlap of 50%, this resulted in a resolution of 1.6 mm for the tethered and 1.7 mm for the free-flight measurements, which is about 10–16% of hindwing chord (C_{HW}) depending on the distance from the wing root. For the measurements performed on tethered specimens that had one forewing removed, the resolution was 1.2 mm, which is about 8–14% of C_{HW} depending on the said distance. The measured flow filed was validated by setting a threshold of 1.3 in the relative peak ratio of the cross-correlation function of the PIV images. Those vectors were considered erroneous and deleted where the relative peak ratio was below 1.3 [Q=(P_1−min)/(P_2−min), where min is the lowest value of the correlation plane and P_1 and P_2 are the heights of the highest and second-highest correlation peaks]. In the final pass, the applied median filter computes a median vector from neighboring vectors and compares the middle vector with this median vector ±deviation of the closest neighboring vectors. The center vector was rejected if its magnitude was greater than or equal to three times the neighborhood root mean square (rms); the filter replaced first-choice vectors with second-, third- or fourth-choice vectors if their magnitude was less than twice the neighborhood rms. The removed vectors, which typically occupied less than 5% of the entire vector field, were interpolated using their neighboring vectors. The velocity (and vorticity) uncertainties were 0.0016 m s^{-1} (1.91 s^{-1}), 0.0013 m s^{-1} (1.54 s^{-1}) and 0.0018 m s^{-1} (2.96 s^{-1}) for measurements performed on tethered specimens, free-flight specimens and tethered specimens with one of their forewings cut off, respectively.

Circulation calculation

LEV circulation was calculated to assess the effect of wing–wing interactions on different parts of the wing. LEV circulation at a given measurement cross-section is proportional to the force acting in the direction normal to the wing surface that is produced along that cross-section by the LEV according to the Kutta–Joukowski theorem. Thus, it can be used as a direct indicator of aerodynamic performance (Van Den Berg and Ellington, 1997). To quantify the interaction effect on the hindwing, its LEV circulation was calculated according to the method described in Fu et al. (2014, 2017). The vortex region was identified using the λ_{ci} method from Zhou et al. (1999) by setting the threshold at 10% of the maximum vorticity. The location of the hindwing LEV core could be identified within the measurement area to exclude alien vortex entities of the same spin from the calculation.

Measurement of wing kinematics

The flapping wing parameters can be determined by the pterostigma and the wing root positions on the recorded PIV frames, using the known distance between the pterostigma and the wing root of the specimens. The PIV images ensure easy identification of the pterostigma throughout the whole flight sequence. The mean amplitude of the positional angles (ϕ) of the wings of the tethered specimens represents the average of eight flapping cycles. The pterostigma was traced manually with a precision of ±3 pixels, resulting in a positional angle uncertainty of ±0.5 deg. From the time histories of the positional angle, the flapping frequency and phasing were determined using a five-point fitting interpolation fast Fourier transform (FFT) algorithm and a cross-spectral density technique (Qiu et al., 1991). The uncertainty of the frequency with a 95% confidence level was below ±0.2 Hz and the uncertainty of the calculated phasing was ±1 deg. As the exact location of the wing root could not be pinpointed in the low-resolution raw PIV images, we could not determine the positional angles from the free-flight flow measurements, but we could estimate other kinematic parameters.

RESULTS

Behavior of tethered and free-flying dragonflies

The kinematic parameters of seven tethered and seven free-flying dragonflies were recorded for a representative flight of 8 flapping cycles each (Table S1). Table 1 summarizes the mean kinematic parameters and the variances. While tethered, the flapping frequency, wing phasing and stroke-plane angle averaged 24.4 Hz, 82 deg and 64 deg, respectively. The mean of the amplitudes of the forewing and hindwing positional angles were the same, i.e. 65 deg. The mean of the baseline of the positional angle of the forewing was on the dorsal side (+6.8 deg), while that of the hindwing was at 0 deg, implying a 6.8 deg ventral offset.

Journal of Experimental Biology (2018) 221, jeb171199. doi:10.1242/jeb.171199

The measured kinematic parameters were almost the same after one of the forewings was cut off.

In free flight, the estimated mean values of flapping frequency, wing phasing and stroke-plane angle were 36.3 Hz, 92 deg and 64 deg, respectively. The average flight speed of the specimens was 1.7 m s^{-1}, which is a moderate speed considering that dragonflies can reach 10 m s^{-1} when hunting or fleeing. The estimated values are within a reasonable range. Also, in free flight, the majority of specimens did not follow a straight flight path, but alternated between ascending and descending, and occasionally accelerated and decelerated, which explains the differences between free-flight and tethered measurements.

The angle between the leading edge of the forewing and that of the hindwing (defined as the wing separation angle) produced during an upstroke was much smaller than that produced during a downstroke (see Figs 1A and 2C). The large difference results from the offset between the baselines of the forewing and hindwing (ϕ) during a flapping cycle (Movies 1 and 3). The implications of this asymmetry will be evaluated in the Discussion.

Fig. 2 shows the measured velocity field (Fig. 2A), the pterostigma trajectory (Fig. 2B) and the positional angle of the wings for three flapping cycles (Fig. 2C), together with the definition of stroke plane angle and baseline offset. The tethered specimen generated a momentum in the horizontal direction (as shown by the velocity flux in Fig. 2A). The horizontal component of the momentum propels horizontal forward flight if the dragonfly is not tethered, while the vertical component contributes to weight support. This behavior was the most representative of tethered

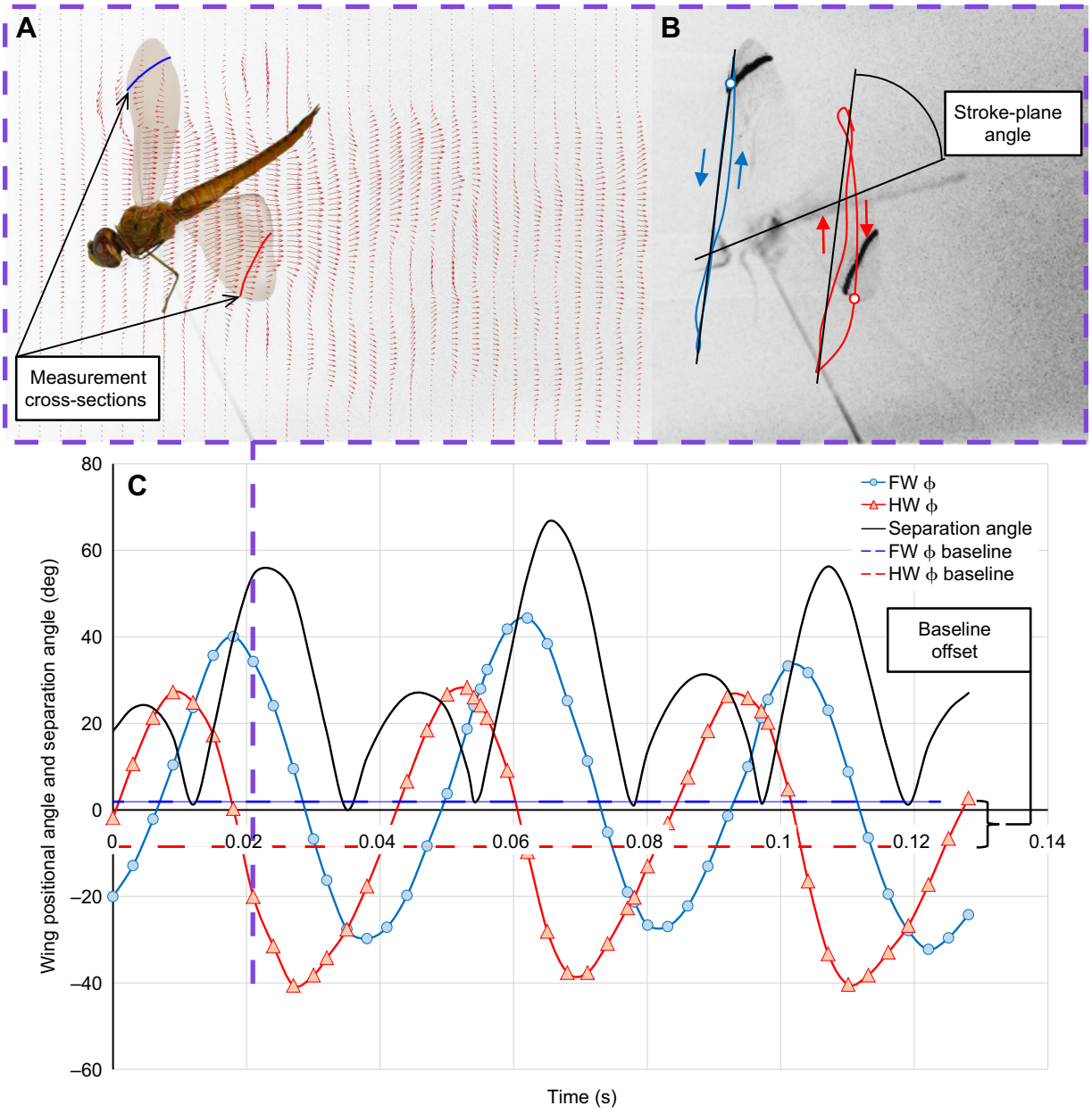

Fig. 2. Results of a representative flow measurement in tethered flight. (A) Instantaneous velocity field in the outer region of the wings. (B) The trajectories of the pterostigma of the forewing (blue line) and hindwing (red line) together with the stroke-plane angle. The two white dots mark the locations of the pterostigma. (C) Wing positional angle (ϕ), baselines of the positional angles and the wing separation angle for three flapping cycles. FW, forewing; HW, hindwing.

Journal of Experimental Biology (2018) 221, jeb171199. doi:10.1242/jeb.171199

measurements, and there was no obvious change in the flapping pattern across the flapping cycles during each flight measurement. Fig. 2A,B shows the tethered dragonfly deliberately tilted at an angle to aid visualization.

Spanwise variance of flow

Based on the qualitative flow features derived from flow measurements for tethered flight, four distinct regions of the wing were found for the typical case of quarter-cycle hindwing-led phasing. Fig. 1B shows the four regions: the root region (i.e. the 12% portion that is closest to the wing root, shaded in red), the inner region (i.e. the portion between the 12% line and the 36% line, shaded in yellow), the transition region (i.e. the portion between the 36% line and the 60% line, shaded in green) and the outer region (i.e. the remaining portion that is also the farthest from the wing root, shaded in purple). In Fig. 3 and in the figures that follow, wing motion is indicated by bold black arrows; straight arrows denote upstrokes or downstrokes and curved arrows denote upward or downward pitching at stroke reversal. During pitching, the leading and trailing edges of a wing move in opposite directions. Furthermore, in the figures presenting the flow fields, F and H refer to vortexes formed by the forewing and the hindwing, respectively, while D and U refer to vortexes formed during the downstroke and the upstroke, respectively. Additionally, asterisks mark a captured vortex. Figs 3–5 present the measurement results rotated to horizontal body orientation to help interpret the results in a natural physiological body posture of the flight. The effects of interwing interaction were qualitatively similar across all seven tethered specimens. Figs 7–9 present the flow measurement results in the tethered condition.

Root region

Because of the combined wall effect resulting from the body and the small positional displacement of the wings, the wing root region

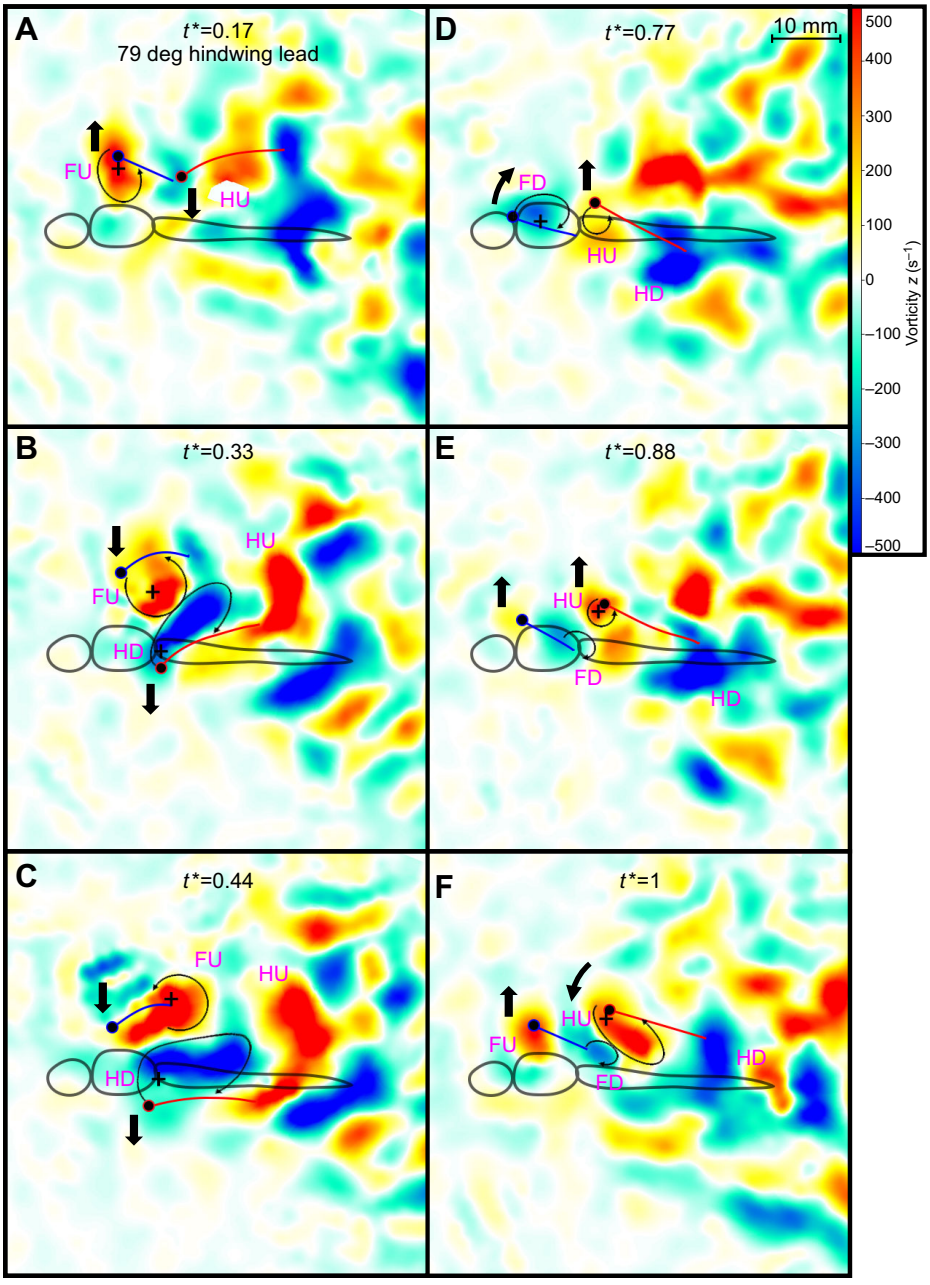

Fig. 3. Main flow features in the inner region (at 18% of S_{HW} from the wing root) throughout a complete flapping cycle in tethered flight. (A–C) The synergistic leading-edge vortex–leading-edge vortex (LEV–LEV) interaction (between forewing upstroke FU and hindwing downstroke HD) while the hindwing is downstroking. (D–F) The synergistic LEV–LEV interaction (between forewing downstroke FD and hindwing upstroke HU) while the hindwing is upstroking. Wing motion and vortex rotation are indicated by arrows; t^*=0 marks the time when the hindwing commences its downstroke. Here and in subsequent figures, the plus signs in the figures indicate the positions of a vortex core given that it could be clearly located in the measured flow fields.

Journal of Experimental Biology (2018) 221, jeb171199. doi:10.1242/jeb.171199

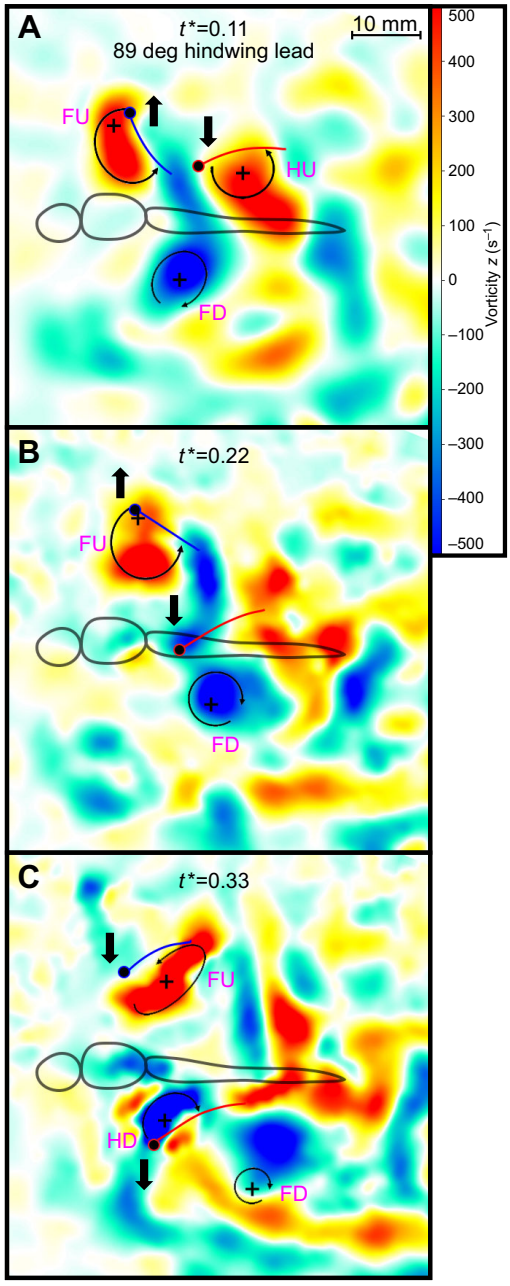

Fig. 4. Main flow features in the transition region (at 42% of S_{HW} from the wing root) while the hindwing is downstroking in tethered flight. (A) The hindwing commences the downstroke by moving toward the vortex shed by the forewing (FD). (B) The vortex shed by the forewing (FD) located downstream below the translating hindwing and not interacting with it. (C) Delayed formation of the hindwing LEV (HD). The vortex shed by the forewing (FD) dissipates downstream. Wing motion and vortex rotation are indicated by arrows; t^*=0 marks the time when the hindwing commences its downstroke.

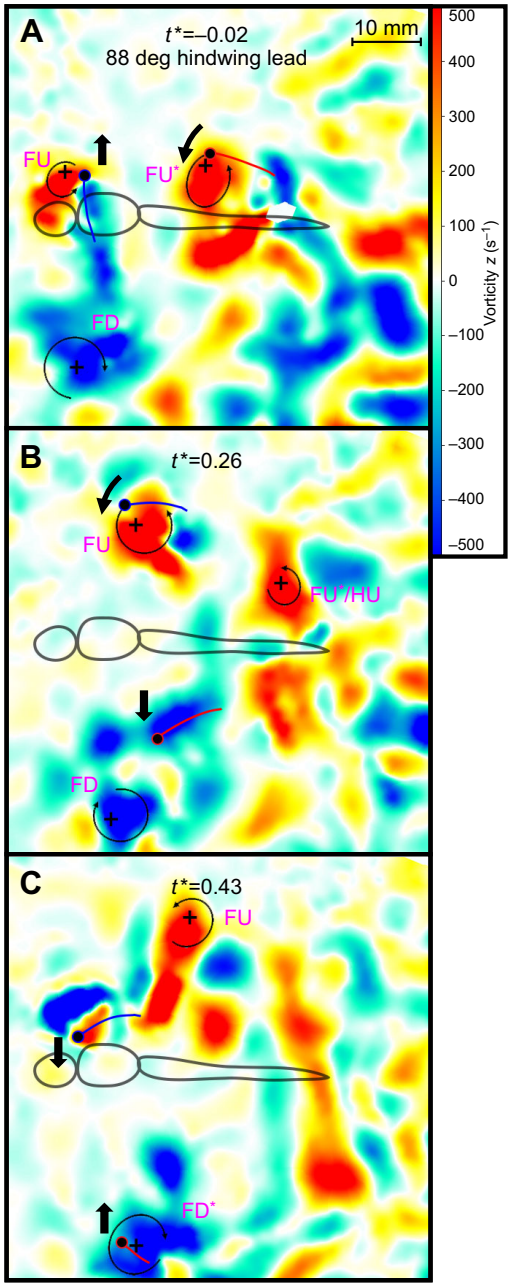

Fig. 5. Main flow features in the outer region (at 78% of S_{HW} from the wing root) while the hindwing is downstroking in tethered flight. (A) The hindwing is pitching downward. The LEV (FU*) formed with the help of forewing's vortex capture is pulled downstream by the changing pressure gradient along the wing's bottom side. (B) The hindwing translates toward the vortex shed by the forewing (FD). No hindwing LEV is formed. (C) The hindwing captures the vortex shed by the forewing (FD*). Wing motion and vortex rotation are indicated by arrows; t^*=0 marks the time when the hindwing commences its downstroke.

exhibited the least aerodynamic performance. The leading edge of the forewing guided and distributed the incoming flow while forming a weak LEV. The hindwing, however, did not generate a LEV. A TEV was created by the pitching motion of the hindwing. The upstroke and downstroke counter-rotating hindwing TEVs formed a narrow, reverse von Kármán vortex street that induced a streamwise jet. Fig. S1 shows the flow field and the hindwing-shed TEVs.

Inner region

We describe the flow features of the inner region based on the measurement taken from the 18% cross-section in Fig. 1B (i.e. at 18% of S_{HW} from the wing root). As shown in Fig. 3A,D, at t^*=0.17 and 0.77, the hindwing leading edge and the forewing trailing edge move in opposite directions. In Fig. 3A, the hindwing leading edge moves downward while the forewing trailing edge moves upward. Similarly, in Fig. 3D, the forewing is pitching upward during the

Journal of Experimental Biology (2018) 221, jeb171199. doi:10.1242/jeb.171199

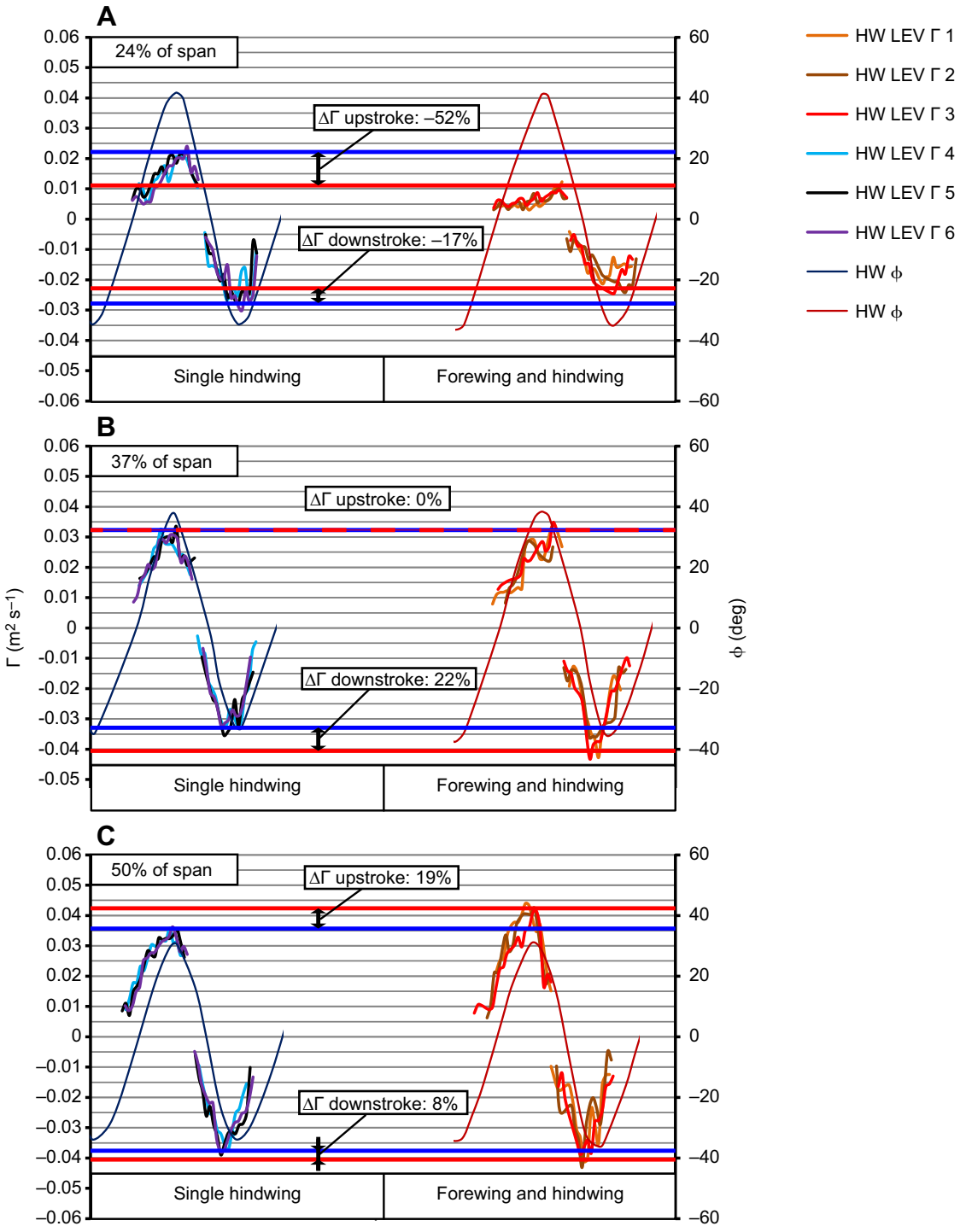

Fig. 6. Hindwing LEV circulation over three flapping cycles at three measurement cross-sections in tethered flight. Blue curves show the circulation (Γ) in the case of a single hindwing; red shows values including the effect of the forewing. The blue straight lines indicate the maximum values of the single-hindwing circulation obtained by averaging the maximum values of the three flapping cycles measured. Similarly, the red straight lines indicate the maximum values of the hindwing circulation in the tandem-wing configuration obtained by averaging the maximum values of the three flapping cycles measured. ΔΓ represents the circulation difference between the hindwing operating solo and in tandem with the forewing, taking the solo operation values as reference. The circulation curves are moved to the same starting position to aid in their comparison. The hindwing positional angle is added for easier interpretation of the flapping cycle. (A) 24% of S_{HW}; (B) 37% of S_{HW}; and (C) 50% of S_{HW} from the wing root. ϕ, wing positional angle.

initial stage of the upstroke. During upward pitching, the forewing trailing edge moves downward while the hindwing leading edge moves upward. With the leading edge of the hindwing in close proximity to the trailing edge of the forewing, the opposite wing movement and the forewing LEV together facilitate the formation of a LEV on the hindwing. The hindwing LEV that is formed during the downstroke (HD) is visible in Fig. 3B,C and the hindwing LEV formed during the upstroke (HU) can be seen in Fig. 3D–F. As the

Journal of Experimental Biology (2018) 221, jeb171199. doi:10.1242/jeb.171199

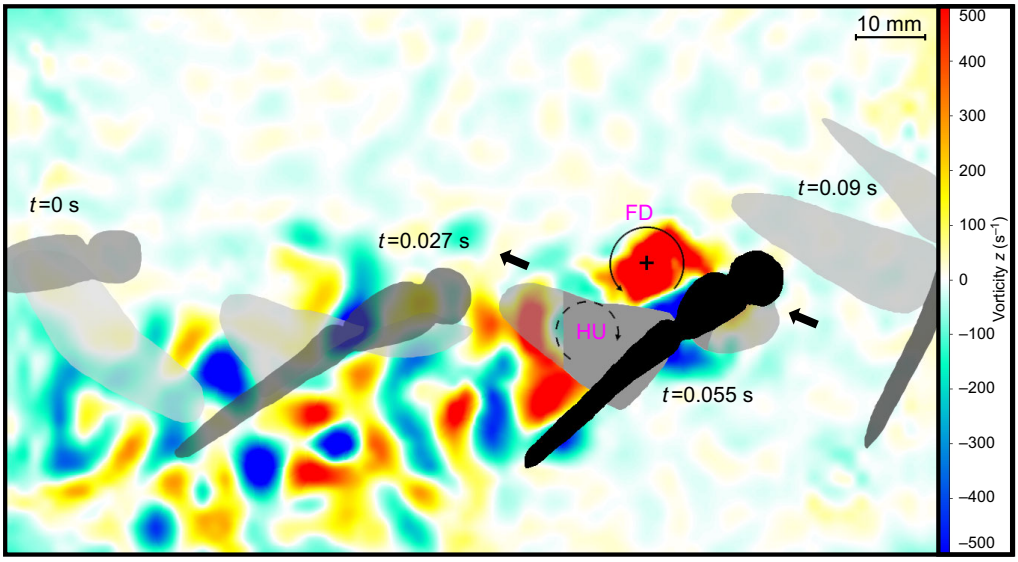

Fig. 7. Free-flight flow measurement in the inner region showing the downstroke forewing LEV (FD) affecting the upstroking hindwing. For easier interpretation of the flight path, the dragonfly silhouette is also shown for various time instants with t=0 s referring to the time at which the dragonfly enters the measurement field of view from the far left. Wing motion and vortex rotation are indicated by arrows. The assumed position of the hindwing LEV formed during the upstroke (HU) is shown by the dashed line.

stroke progresses at t^*=0.33 and 0.88 (Fig. 3B,E), the forewing LEV and the hindwing LEV interact with each other. The LEV of the forewing (FD in Fig. 3D–F and FU in Fig. 3A–C) induces a flow that transfers energy to the shear layer of the hindwing LEV. Boosted by the interaction, the hindwing LEV blocks and redirects the shedding of the forewing LEV.

The shedding of the forewing LEV and that of the hindwing LEV are synchronized as shown in Fig. 3B,C as well as Fig. 3E,F. During the final stage of the stroke at t^*=0.44 and 1.0 (see Fig. 3C,F), the hindwing LEV further expands downstream and covers the entire wing surface without detaching from it. Eventually, this LEV follows the changing pressure gradient at stroke reversal and forms the starting vortex of the next cycle. Movie 1 shows the measured flow field.

Transition region

We present the flow features of the transition region based on the measurement taken from the 42% cross-section in Fig. 1B (i.e. at 42% of S_{HW} from the wing root). Fig. 4A shows the forewing LEV (FU) as the wing approaches the end of the upstroke while the TEV (FD) detaches early on in the upstroke. The detached forewing TEV (FD) is shed below the hindwing during its downstroke (Fig. 4A). However, as the hindwing stroke progresses, it does not capture this forewing-shed TEV (FD in Fig. 4B). Despite having no direct interaction with the shed vortex, the hindwing moves through the flow induced by the forewing, which has a substantial streamwise component. This streamwise flow reduces the effective angle of attack of the hindwing and suppresses LEV formation. A hindwing LEV (HD) is formed, albeit delayed, as the hindwing moves through this region, as shown in Fig. 4C. A hindwing LEV (HU) is formed during the upstroke in an analogous manner and can be seen in Fig. 4A. The flow features of the transition region are presented in Movie 2.

Outer region

We present the flow features of the outer region based on the measurement taken from the 78% cross-section in Fig. 1B (i.e. at 78% of S_{HW} from the wing root). Fig. 5A shows the forewing approaching the upstroke extreme position. Its LEV (FU) is attached while the TEV (FD) has shed earlier at the beginning of the stroke. The LEV of the forewing starts to shed as the forewing is pitching downward at the end of the upstroke (Fig. 5B). The forewing LEV is pulled by the changing pressure gradient of the stroke reversal and moves from the leading edge to the trailing edge of the forewing, where it detaches from the wing. After detaching from the trailing edge, the shed vortex remains intact as shown in Fig. 5A (vortex FD) and Fig. 5C (vortex FU). In Fig. 5B, we can see that the hindwing moves through the region dominated by the flow induced by the forewing. Similar to the situation in the transition region, this flow decreases the effective angle of attack of the hindwing, resulting in an attached flow. As the hindwing reaches the end of its stroke, the separation distance between the outer region of the forewing and that of the hindwing and their flap phasing relationship enable the hindwing to interact with the forewing-shed vortex (FD in Fig. 5A–C). Fig. 5C shows the hindwing capturing this shed vortex with its suction surface to form an enhanced LEV (FD* in Fig. 5C) during the last quarter of the stroke. In Fig. 5A,C, it can also be seen that the dynamic cambering of the flexible membrane of the hindwing in the rotational phase envelops the captured vortex. The hindwing captures a vortex during the upstroke in an analogous manner. A forewing LEV (FU*) captured during the upstroke can be seen in Fig. 5A. Movie 3 shows the flow field measured in the outer region.

Effect of vortex synergy

A forewing-shed vortex can either strengthen or attenuate the formation of a LEV on the hindwing. We conducted a series of measurements across the span of the wings of tethered specimens, first with both forewings intact, then with one of the forewings removed. Based on the flow measurement results of a representative specimen, we calculated the LEV circulation of the hindwing along three cross-sections of the wing, i.e. at 24%, 37% and 50% of S_{HW} from the wing root (Fig. 6A–C). In the case of this representative specimen, synergy is identified between the forewing LEV and the hindwing LEV along these cross-sections. In Fig. 6A–C, the circulations of three flapping cycles are compared at different positional angles of the hindwing.

At 24% of S_{HW} (Fig. 6A), because the separation between the translating wings during the upstroke of the hindwing is so small, the hindwing LEV is suppressed by the interaction. The maximum circulation (Γ) for a single hindwing during the upstroke is 0.022 $m^2\ s^{-1}$ but it is down to 0.011 $m^2\ s^{-1}$ for tandem wings.

Journal of Experimental Biology (2018) 221, jeb171199. doi:10.1242/jeb.171199

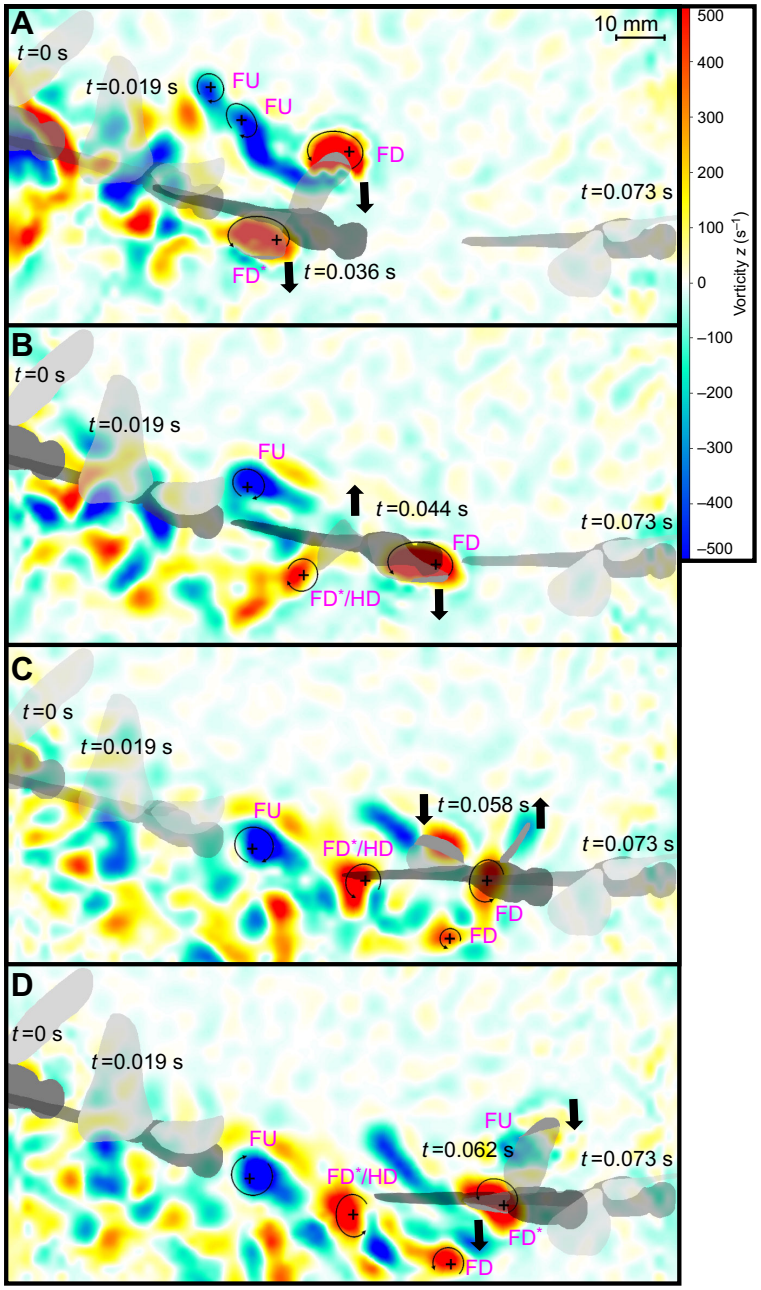

Fig. 8. Free-flight flow measurement in the outer region. (A,B) The hindwing is upstroking. It fails to capture the vortex shed by the forewing (FU). (C,D) The hindwing is downstroking. It captures the vortex shed by the forewing (FD). For easier interpretation of the flight path, the dragonfly silhouette is also shown for various time instants, where *t*=0 s refers to the time at which the dragonfly enters the measurement field of view from the far left. Wing motion and vortex rotation are indicated by arrows.

Similarly, during the downstroke, the maximum circulation for a single hindwing is -0.028 m^2 s^{-1} but it drops to -0.023 m^2 s^{-1} for tandem wings. Hindwing circulation is not enhanced in any way at 24% of $S_{HW.}$ At 37% of S_{HW} (Fig. 6B), the maximum circulation during the downstroke of the hindwing shows a significant, 22% enhancement from -0.033 m^2 s^{-1} to -0.041 m^2 s^{-1} for tandem wings although it remains almost unchanged (0.034 m^2 s^{-1}) during the upstroke. At 50% of S_{HW} (Fig. 6C), the maximum circulation during the upstroke of the hindwing receives a 19% boost (from 0.036 m^2 s^{-1} to 0.043 m^2 s^{-1}). The downstroke maximum circulation is also improved by 8% (from -0.038 m^2 s^{-1} to -0.041 m^2 s^{-1}).

Free-flight flow measurements

It is important to assess how representative the flow features observed in tethered flight experiments are of those displayed during unrestricted flight. We conducted free-flight measurement on the same species of live dragonflies to support the findings presented above. Ensuring that measurements are taken from precise locations of the wing is difficult when working with free-flying specimens. Nevertheless, the four regions that we identified above are wide enough for us to be able to determine to which region a particular free-flight measurement belongs. In the successful measurements of all seven specimens in free flight we observed seven flights showing the forewing LEV interacting with the hindwing in the inner region and seven flights with vortex capturing in the outer region. Two measurement results which are representative of the successfully captured flights are discussed below.

Fig. 7 presents a free-flight measurement in the inner region, as the dragonfly reoriented its body before ascending. A strong forewing downstroke LEV (FD in Fig. 7) can be seen close to the leading edge of the upstroking hindwing. From this observation, we can assume that the flow induced by the forewing LEV affects the

Journal of Experimental Biology (2018) 221, jeb171199. doi:10.1242/jeb.171199

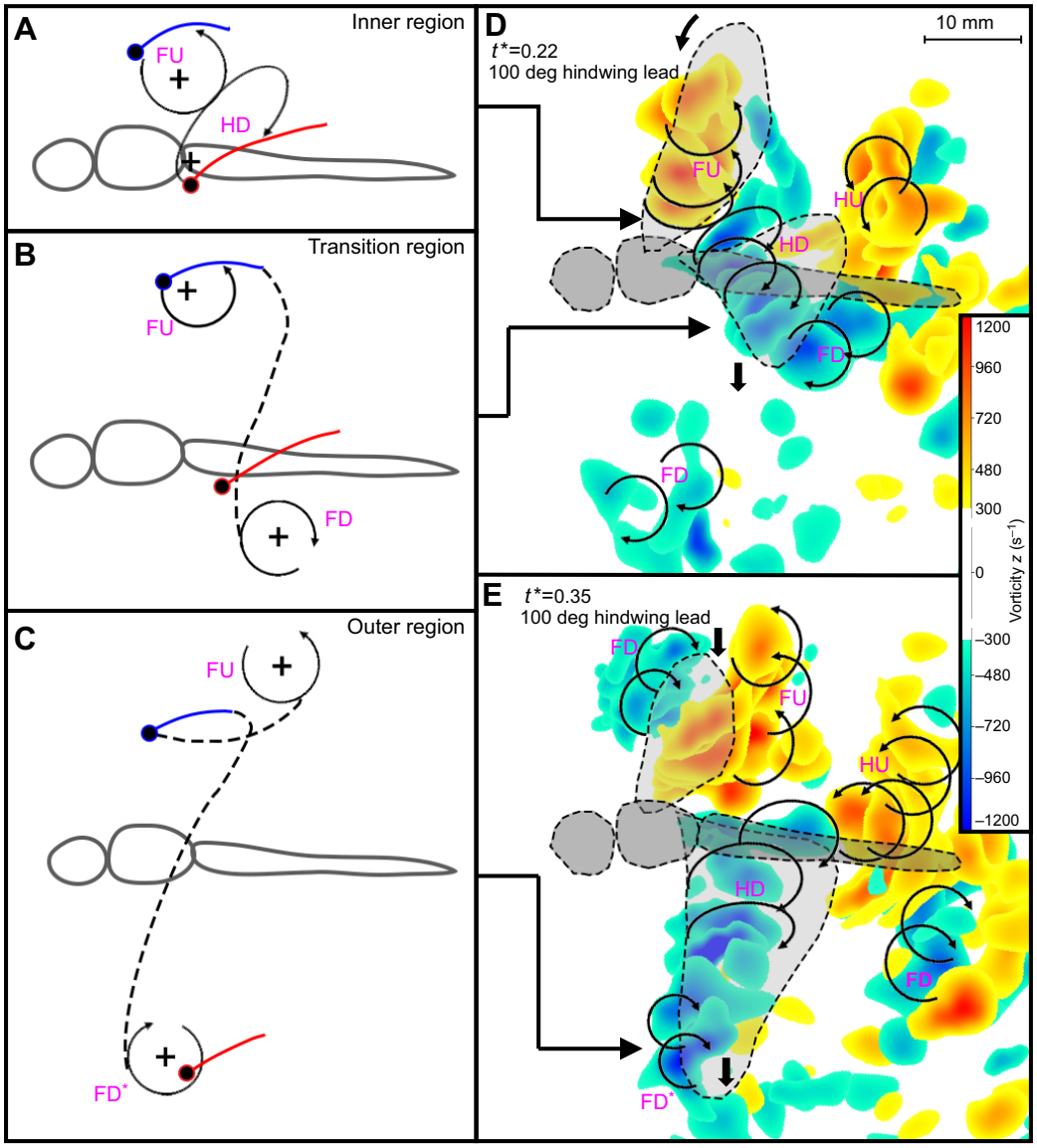

Fig. 9. Schematic diagram of the flow features across the span of the wing in tethered flight. (A) Schematic diagram of the vortex synergy in the inner region and (B) shedding of the forewing vortex downstream below the hindwing in the transition region. (C) Schematic diagram of the vortex capture in the outer region. In B and C, the dashed lines connect the vortex to the wing from which it is shed. (D) Strong vorticity zones across the span of the wing indicate the formation of vortexes half-way through the downstroke of the hindwing. The vortex synergy in the inner region is observable at this time instant. (E) Strong vorticity zones across the span of the wing indicate the formation of vortexes at the end of the downstroke of the hindwing. The wake vortex capture is observable at this time instant. Wing motion and vortex rotation are indicated by arrows.

hindwing strongly and could transfer energy to the shear layer of the leading edge of the hindwing. The hindwing covers the area where its clockwise-rotating LEV would form. Fig. 8 shows vortex capture in the outer region containing the wing tip in the case of descending flight. No vortex was captured during the upstroke (Fig. 8A,B). It was only captured during the downstroke of the hindwing (Fig. 8A,C,D).

Vortex positioning in 3D space during the interaction

Finally, to aid in interpreting the presented results in 3D space, Fig. 9 shows the measured flow fields seen from one of the PIV cameras at two time instants: t^*=0.22 and t^*=0.35. Only the strong vortical structures are displayed in the figure so that we can show all of the overlapping measurement cross-sections. At t^*=0.22 (Fig. 9A,B,D), vortex synergy can be observed in the inner region. At t^*=0.35 (Fig. 9C,E), vortex capture in the outer region is obvious.

DISCUSSION

LEV–LEV interaction in the inner region

As shown in Fig. 3, the forewing LEV is in close proximity to the hindwing LEV in the inner region, resulting in a synergistic interaction during both the downstroke (between the vortexes FU and HD in Fig. 3B,C) and the upstroke (between FD and HU in Fig. 3E,F) of the hindwing. This kind of LEV–LEV interaction was also found in the free-flight condition as shown in Fig. 7. While the wings are flapping, the distance between the leading edge of the forewing and that of the hindwing plays an important role in the formation of the hindwing LEV. At 24% of S_{HW} in the inner region, because the distance between the translating wings is small

(see Figs 1A,B and 9), the forewing trailing edge is very close to the hindwing leading edge (Fig. 1B), which may suppress the formation of the hindwing LEV. Consequently, the circulations of the hindwing LEV are reduced by 52% for the upstroke and 17% for the downstroke compared with the hindwing-only condition as shown in Fig. 6A (24% of S_{HW}). The asymmetric reduction is attributed to the different wing distances during the upstroke and the downstroke due to the offset between the baselines of the forewing and hindwing.

At 37% of S_{HW}, the distance between the wings is larger, allowing the forewing LEV to promote the circulation of the hindwing LEV by 122% over the hindwing-only condition during the downstroke (Fig. 6B). Near midspan (Fig. 6C), the separation between the wings and their LEVs increases and it is too large for a strong LEV–LEV synergy (see Figs 1A,B and 9), the LEV–LEV interaction resulting in only an 8% enhancement of the hindwing LEV circulation during the downstroke. In contrast, as the hindwing flaps closer to the ventral side than does the forewing, the distance between the two wings is smaller during the upstroke, allowing a 19% enhancement of the maximum hindwing LEV circulation (Fig. 6C). It is clear that the distance between the forewing and the hindwing increases gradually in the direction towards the wingtip, which diminishes the synergistic interactions between their LEVs.

Zheng et al. (2016a) presented a similar interaction scenario in forward flight using rigid robotic wings. However, in their study, the wings could only perform pitching and plunging motion. Therefore, the distance between the forewing and hindwing was always the same, resulting in similar flow structures across the span of the wings. Their system was thus different from a natural dragonfly flapping-wing system, which is in fact a root-flapping tandem-wing system.

A rigid wing can induce a strong TEV. The TEV of the forewing can interact with the LEV of the hindwing (Maybury and Lehmann, 2004; Hsieh et al., 2010; Rival et al., 2011; Broering et al., 2012; Hu and Deng, 2014; Xie and Huang, 2015; Zheng et al., 2016a). This kind of TEV–LEV interaction can also strengthen the hindwing LEV. A dragonfly wing is flexible and its shape is the result of the dynamic balance between the wing's inertia, stiffness and the aerodynamic force exerted on it (Combes and Daniel, 2003a,b; Kang et al., 2011). A compliant wing adapts its shape to the flow field and does not shed as much vorticity from the trailing edge as a rigid wing does (Heathcote and Gursul, 2007; Fu et al., 2018). Hence, a flexible wing has less trailing edge-induced vorticity, allowing sufficient space for the forewing LEV and the hindwing LEV to interact.

In natural dragonflies, the LEV of each wing starts to shed along the wing surface while the wing is pitching at the end of a stroke (see Figs 3B,D, 4C and 5B for the shedding forewing LEV and Figs 3A, 4A and 5A for the shedding hindwing LEV; see also Movies 1–3). The LEVs after stroke reversal would be quickly broken down by the translational motion of a rigid wing (Maybury and Lehmann, 2004), while a new LEV–TEV pair would be formed by the next stroke. In contrast, a compliant wing membrane would envelop the shedding LEV (Figs 3B and 4A) on the pressure side that is moving towards the trailing edge and initiate TEV formation of the next stroke. This is also the reason that the forewing LEV and the hindwing LEV can interact in dragonflies to promote hindwing LEV circulation.

Transition region

About half-way between the wing root and wing tip lies a transition region where the flow is typically attached to the hindwing (Fig. 4). This is because in tandem operation, the forewing induces a downwash flow that results in a lower effective angle of attack of the hindwing, thus delaying or even suppressing the formation of the LEV (Maybury and Lehmann, 2004; Sun and Lan, 2004; Hu and Deng, 2014).

Previous work did not connect the forewing downwash effect to any particular region of the wing. Our results show that in the inner region, the wings are operating in close vicinity. Thus, the downwash effect is not significant and the LEV–LEV interaction dominates (Figs 3 and 9). Toward the wing tip, the distance between the flapping wings increases such that the downwash interaction effect gradually dominates the vortex interactions (Fig. 9).

We also observed that the transition region can exhibit features similar to those seen in the inner and outer regions following a slight change in the flapping of the specimens. The hindwing might generate a LEV on its own (such as the one formed with some delay following the downstroke in Fig. 4C), or it might capture the TEV shed by the forewing from the previous stroke.

Vortex capture in the outer region

In the outer region, the formation of the hindwing LEV is delayed or even suppressed by the downwash effect (Fig. 5). The hindwing, however, is able to form a LEV in the last quarter of the stroke via vortex capture (Fig. 5C). This vortex capture is essentially different from wake capture, in which the wing utilizes the flow of its own vortical structures shed during stroke reversal (Dickinson et al., 1999; Birch and Dickinson, 2003; Lehmann et al., 2005). Vortex capture could provide a useful aerodynamic force and a momentum that eases the pitching motion of the wing (Lehmann, 2015). Hsieh et al. (2010) also reported vortex capture while the wings were counter-stroking. However, in their 2D numerical study, the TEV shed by the forewing was captured by the hindwing. Because of this interaction, the hindwing lift was boosted to 109% of the single-wing maxima for a short period of time at the end of the upstroke (Hsieh et al., 2010). Zheng et al. (2016a) also showed that the counter-stroking hindwing can capture and utilize the TEV of the forewing during forward flight. In their study, the forewing TEV was captured about half-way through the stroke. They found that the vortex capture generated a force that was as high as that from the LEV–LEV interaction (about 39%) in the case of 90 deg wing phasing (Zheng et al., 2016a). This suggests that vortex synergy and vortex capture could be equally important tools for dragonflies that can result in comparable force gains. Xie and Huang (2015) also observed vortex capture at 135 and 270 deg phasing. Different from the current findings, however, the vortex shed by the forewing interacted with the hindwing after its stroke reversal and induced the formation of a new LEV during the next stroke. Xie and Huang (2015) used 2D modeling and linked the interaction scenarios to the effect of wing phasing but not to the different regions of root-flapping wings. Our results indicate that the hindwing can be made to fully capture the vortex shed by the forewing and to anchor it to its suction side in the case of 90 deg hindwing-led phasing (Fig. 5).

Effect of the offset between wing positional angles, and effect of flight direction

Regarding the vortex capture in the outer region, because the hindwing flaps closer to the ventral side it is closer to the vortex shed by the forewing during the downstroke than during the upstroke. Consequently, vortex capture occurs earlier during the downstroke than during the upstroke. The vortex is anchored by the hindwing for a longer period of time to provide a greater aerodynamic force. Additionally, the free-flight flow field measurements shown in

Fig. 8 suggest that the successful capture of a vortex in the outer region is also dependent on the flight direction. For example, in descending flight shown in Fig. 8, the vortex that is shed by the forewing above the dragonfly (FU in Fig. 8A,B) moves away from the direction of flight so that the hindwing is less able to capture and utilize it during its upstroke. In the case of descending flight, the downstroking hindwing is more likely to capture the vortex that is shed by the forewing below the dragonfly (FD in Fig. 8A,C,D) as it flies towards it.

Conclusion

We investigated the spanwise variance in the interwing interaction of dragonflies *in vivo*. Measurements on tethered specimens in still air, which simulates hovering and slow forward flight, were evaluated and we report for the first time a distinct LEV–LEV synergy in the inner region of the wing (i.e. the region that is away from the wing root but not quite up to midspan), which can boost the circulation of the hindwing LEV by as much as 22%. An essentially different interaction scenario was observed in the region farthest from the wing root (i.e. the outer region). Here, the ingenious phasing and instinctive control of the wings render the capture of the forewing wake vortex possible.

The angle between the flapping wings undergoes periodic variation as a result of a ventral (or dorsal) offset of the hindwing flapping positional angles, resulting in different intensities of the reported interaction features in the upstroke and the downstroke. Further parametric studies are necessary to evaluate how such control is implemented in tandem flapping wing flyers.

With recent advancements in materials science and microfabrication techniques, it has become feasible to design artificial insect wings with non-uniform flexibility. Characterizing the spanwise functionality of dragonfly wings can help optimize the regional flexibility of artificial wings to better exploit interwing interaction features. We hope that the results presented here will inspire the design of micro-air vehicles with improved flapping wing locomotion.

Competing interests

The authors declare no competing or financial interests.

Author contributions

Conceptualization: C.H., H.Q., W.S.; Methodology: C.H., H.Q.; Validation: C.H.; Formal analysis: C.H., W.S.; Investigation: C.H.; Resources: H.Q.; Writing - original draft: C.H.; Writing - review & editing: C.H., H.Q., W.S.; Visualization: C.H.; Supervision: H.Q., W.S.; Project administration: H.Q.; Funding acquisition: H.Q.

Funding

This research was supported by the Hong Kong PhD Fellowship Scheme from the Research Grants Council, University Grants Committee, the Government of the Hong Kong Special Administrative Region (HKSAR) and the Hong Kong University of Science and Technology.

Supplementary information

Supplementary information available online at
http://jeb.biologists.org/lookup/doi/10.1242/jeb.171199.supplemental

References

Alexander, D. E. (1984). Unusual phase relationships between the forewings and hindwings in flying dragonflies. *J. Exp. Biol.* **109**, 379-383.
Azuma, A. and Watanabe, T. (1988). Flight performance of a dragonfly. *J. Exp. Biol.* **137**, 221-252.
Birch, J. M. and Dickinson, M. H. (2003). The influence of wing-wake interactions on the production of aerodynamic forces in flapping flight. *J. Exp. Biol.* **206**, 2257-2272.
Birch, J. M., Dickson, W. B. and Dickinson, M. H. (2004). Force production and flow structure of the leading edge vortex on flapping wings at high and low Reynolds numbers. *J. Exp. Biol.* **207**, 1063-1072.
Bomphrey, R. J., Nakata, T., Henningsson, P. and Lin, H.-T. (2016). Flight of the dragonflies and damselflies. *Phil. Trans. R. Soc. B.* **371**, 20150389.
Broering, M. T., Lian, Y. S. and Henshaw, W. (2012). Numerical investigation of energy extraction in a tandem flapping wing configuration. *AIAA J.* **50**, 2295-2307.
Chin, D. D. and Lentink, D. (2016). Flapping wing aerodynamics: from insects to vertebrates. *J. Exp. Biol.* **219**, 920-932.
Combes, S. A. and Daniel, T. L. (2003a). Flexural stiffness in insect wings. I. Scaling and the influence of wing venation. *J. Exp. Biol.* **206**, 2979-2987.
Combes, S. A. and Daniel, T. L. (2003b). Flexural stiffness in insect wings. II. Spatial distribution and dynamic wing bending. *J. Exp. Biol.* **206**, 2989-2997.
Combes, S. A., Rundle, D. E., Iwasaki, J. M. and Crall, J. D. (2012). Linking biomechanics and ecology through predator–prey interactions: flight performance of dragonflies and their prey. *J. Exp. Biol.* **215**, 903-913.
Dickinson, M. H. and Götz, H. G. (1993). Unsteady aerodynamic performance of model wings at low Reynolds numbers. *J. Exp. Biol.* **174**, 45-64.
Dickinson, M. H., Lehmann, F. O. and Sane, S. P. (1999). Wing rotation and the aerodynamic basis of insect flight. *Science* **284**, 1954-1960.
Ellington, C. P., Van den Berg, C., Willmott, A. P. and Thomas, A. L. R. (1996). Leading-edge vortices in insect flight. *Nature* **384**, 626-630.
Fu, J.-J., Hefler, C., Qiu, H.-H. and Shyy, W. (2014). Effects of aspect ratio on flapping wing aerodynamics in animal flight. *Acta Mech. Sin.* **30**, 776-786.
Fu, J., Shyy, W. and Qiu, H. (2017). Effects of aspect ratio on vortex dynamics of a rotating wing. *AIAA J.* **55**, 1-9.
Fu, J., Liu, X., Shyy, W. and Qiu, H. (2018). Effects of flexibility and aspect ratio on the aerodynamic performance of flapping wings. *Bioinsp. Biomim.* (In press) **13**, 036001. https://doi.org/10.1088/1748-3190/aaaac1.
Heathcote, S. and Gursul, I. (2007). Flexible flapping airfoil propulsion at low Reynolds numbers. *AIAA J.* **45**, 1066-1079.
Hedrick, T. L., Combes, S. A. and Miller, L. A. (2015). Recent developments in the study of insect flight. *Can. J. Zool.* **93**, 925-943.
Hefler, C., Noda, R., Shyy, W. and Qiu, H. (2017). Unsteady vortex interactions for performance enhancement of a free flying dragonfly. *ASME Paper*. FEDSM2017-69579.
Hsieh, C.-T., Kung, C.-F., Chang, C.-C. and Chu, C.-C. (2010). Unsteady aerodynamics of dragonfly using a simple wing-wing model from the perspective of a force decomposition. *J. Fluid Mech.* **663**, 233-252.
Hu, Z. and Deng, X.-Y. (2014). Aerodynamic interaction between forewing and hindwing of a hovering dragonfly. *Acta Mech. Sin.* **30**, 787-799.
Kang, C.-K., Aono, H., Cesnik, C. E. S. and Shyy, W. (2011). Effects of flexibility on the aerodynamic performance of flapping wings. *J. Fluid Mech.* **689**, 32-74.
Lai, G. and Shen, G. (2012). Experimental investigation on the wing-wake interaction at the mid stroke in hovering flight of dragonfly. *Sci. China Phys. Mech. Astron.* **55**, 2167-2178.
Lan, S. and Sun, M. (2001). Aerodynamic force and flow structures of two airfoils in flapping motions. *Acta Mech. Sin.* **17**, 310-331.
Lehmann, F.-O. (2015). When wings touch wakes: understanding locomotor force control by wake–wing interference in insect wings. *J. Exp. Biol.* **211**, 224-233.
Lehmann, F.-O., Sane, S. P. and Dickinson, M. H. (2005). The Aerodynamic effects of wing-wing interaction in flapping insect wings. *J. Exp. Biol.* **208**, 3075-3092.
Maybury, W. J. and Lehmann, F.-O. (2004). The fluid dynamics of flight control by kinematic phase lag variation between two robotic insect wings. *J. Exp. Biol.* **207**, 4707-4726.
Norberg, R. A. (1975). Hovering flight of the dragonfly: Aeschna juncea L., kinematics and aerodynamics. *Swimming and Flying in Nature.* **2**, 763-780.
Qiu, H. H., Sommerfield, M. and Durst, F. (1991). High-resolution data processing for phase-Doppler measurements in a complex two-phase flow. *Meas. Sci. Technol.* **2**, 455-463.
Reavis, M. A. and Luttges, M. W. (1988). Aerodynamic forces produced by a dragonfly. *AIAA Paper* 88-0330.
Rival, D., Schönweitz, D. and Tropea, C. (2011). Vortex interaction of tandem pitching and plunging plates: a two-dimensional model of hovering dragonfly-like flight. *Bioinsp. Biomim.* **6**, 016008.
Rüppell, G. (1989). Kinematic analysis of symmetrical flight manoeuvres of odonatan. *J. Exp. Biol.* **144**, 13-42.
Sane, S. P. (2003). The aerodynamics of insect flight. *J. Exp. Biol.* **206**, 4191-4208.
Shyy, W. and Liu, H. (2007). Flapping wings and aerodynamic lift: the role of leading-edge vortices. *AIAA J.* **45**, 2817-2819.
Shyy, W., Lian, Y., Tang, J., Viieru, D. and Liu, H. (2008). *Aerodynamics of Low Reynolds Number Flyers*. New York, USA: Cambridge University Press.
Shyy, W., Aono, H., Kang, C. K. and Liu, H. (2013). *An Introduction to Flapping Wing Aerodynamics*. New York, USA: Cambridge University Press.
Somps, C. and Luttges, M. (1985). Dragonfly flight–novel uses of unsteady separated flows. *Science* **228**, 1326-1329.
Somps, C. and Luttges, M. (1986). Dragonfly aerodynamics–response. *Science* **231**, 10-10.
Sun, M. and Lan, S. (2004). A computational study of the aerodynamic forces and power requirements of dragonfly hovering. *J. Exp. Biol.* **207**, 887-901.

Thomas, A. L. R., Taylor, G. K., Srygley, R. B., Nudds, R. L. and Bomphrey, R. J. (2004). Dragonfly flight: free-flight and tethered flow visualizations reveal a diverse array of unsteady lift-generating mechanisms, controlled primarily via angle of attack. *J. Exp. Biol.* **207**, 4299-4323.

Usherwood, J. R. and Lehmann, F.-O. (2008). Phasing of dragonfly wings can improve aerodynamic efficiency by removing swirl. *J. R. Soc. Interface.* **5**, 1303-1307.

Van Den Berg, C. and Ellington, C. P. (1997). The three-dimensional leading-edge vortex of a 'hovering' model hawkmoth. *Phil. Trans. R. Soc. Lond. B Biol. Sci.* **352**, 329-340.

Wakeling, J. M. and Ellington, C. P. (1997). Dragonfly Flight. II. Velocities, accelerations, and kinematics of flapping flight. *J. Exp. Biol.* **200**, 557-582.

Wang, Z. J. and Russell, D. (2007). Effect of forewing and hindwing interactions on aerodynamic forces and power in hovering dragonfly flight. *Phys. Rev. Lett.* **99**, 148101.

Wang, H., Zeng, L., Liu, H. and Chunyong, Y. (2003). Measuring wing kinematics, flight trajectory and body attitude during forward flight and turning maneuvers in dragonflies. *J. Exp. Biol.* **206**, 745-757.

Xie, C.-M. and Huang, W.-X. (2015). Vortex interactions between forewing and hindwing of dragonfly in hovering flight. *Theor. Appl. Mech. Lett.* **5**, 24-29.

Yates, G. T. (1986). Dragonfly aerodynamics. *Science* **231**, 10-10.

Zheng, Y., Wu, Y. and Tang, H. (2015). Force measurements of flexible tandem wings in hovering and forward flights. *Bioinsp. Biomim.* **10**, 016021.

Zheng, Y., Wu, Y. and Tang, H. (2016a). An experimental study on the forewing-hindwing interactions in hovering and forward flights. *Int. J. Heat Fluid Flow.* **59**, 62-73.

Zheng, Y., Wu, Y. and Tang, H. (2016b). Time-resolved PIV study on the force dynamics of flexible tandem wings in hovering flight. *J. Fluid. Struct.* **62**, 65-85.

Zhou, J., Adrian, R. J., Balachandar, S. and Kendall, T. M. (1999). Mechanisms for generating coherent packets of hairpin vortices in channel flow. *J. Fluid Mech.* **387**, 353-396.

Table S1. Kinematic parameters of the dragonfly specimens.

Specimen	Flapping frequency [Hz]	Phase difference [deg]	Stroke-plane angle relative to the body [deg]	Forewing Φ amplitude [deg]	Hindwing Φ amplitude [deg]	Baseline of the positional angle of forewing [deg]	Baseline of the positional angle of hindwing [deg]	Average flight speed [m/s]
Dragonfly 1	23.8	87	63	70	69	2	-8.5 (10.5 ventral)	Tethered
Dragonfly 2	24.9	62	60	63	69	5.5	-0,5 (6 ventral)	Tethered
Dragonfly 2	25.4	-	60	-	65	-	-1,5	Tethered (with one forewing removed)
Dragonfly 3	26.7	83	65	62	64	5.5	0.5 (5 ventral)	Tethered
Dragonfly 3	24.6	-	65	-	59	-	2.5	Tethered (with one forewing removed)
Dragonfly 4	24.6	70	64	62	66	12	6 (6 ventral)	Tethered
Dragonfly 4	26.8	-	64	-	66	-	6	Tethered (with one forewing removed)
Dragonfly 5	22.6	85	67	67	61	14.5	8 (6.5 ventral)	Tethered
Dragonfly 5	21	-	67	-	58	-	6	Tethered (with one forewing removed)t
Dragonfly 6	24	109	65	68	68	9	2 (7 ventral)	Tethered
Dragonfly 6	25	-	66	-	71	-	2.5	Tethered (with one forewing removed)
Dragonfly 7	24.5	77	65	62	61	-1	-7,5 (6.5 ventral)	Tethered
Dragonfly 7	26.1	-	63		60	-	-8	Tethered (with one forewing removed)
Dragonfly 8	31	105	70	Indeterminate	Indeterminate	Indeterminate	Indeterminate	1.6
Dragonfly 9	31.4	95	60	Indeterminate	Indeterminate	Indeterminate	Indeterminate	1.6
Dragonfly 10	37	92	66	Indeterminate	Indeterminate	Indeterminate	Indeterminate	1.2
Dragonfly 11	47	75	61	Indeterminate	Indeterminate	Indeterminate	Indeterminate	1.2
Dragonfly 12	37	90	68	Indeterminate	Indeterminate	Indeterminate	Indeterminate	1.7
Dragonfly 13	35	85	62	Indeterminate	Indeterminate	Indeterminate	Indeterminate	3
Dragonfly 14	35.5	100	60	Indeterminate	Indeterminate	Indeterminate	Indeterminate	1.5

Journal of Experimental Biology • Supplementary information

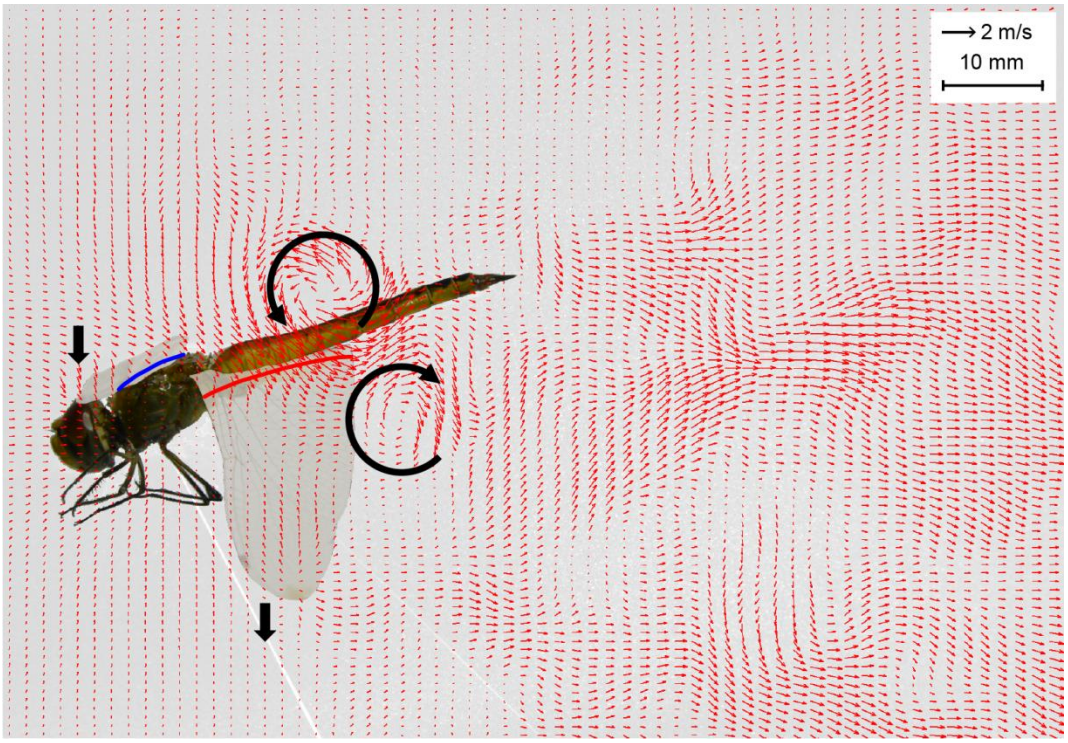

Fig. S1. Flow features of the root region. No hindwing LEV formation. The trailing edge of the hindwing generates a TEV in each stroke that forms a reverse von Kármán vortex street behind the wing.

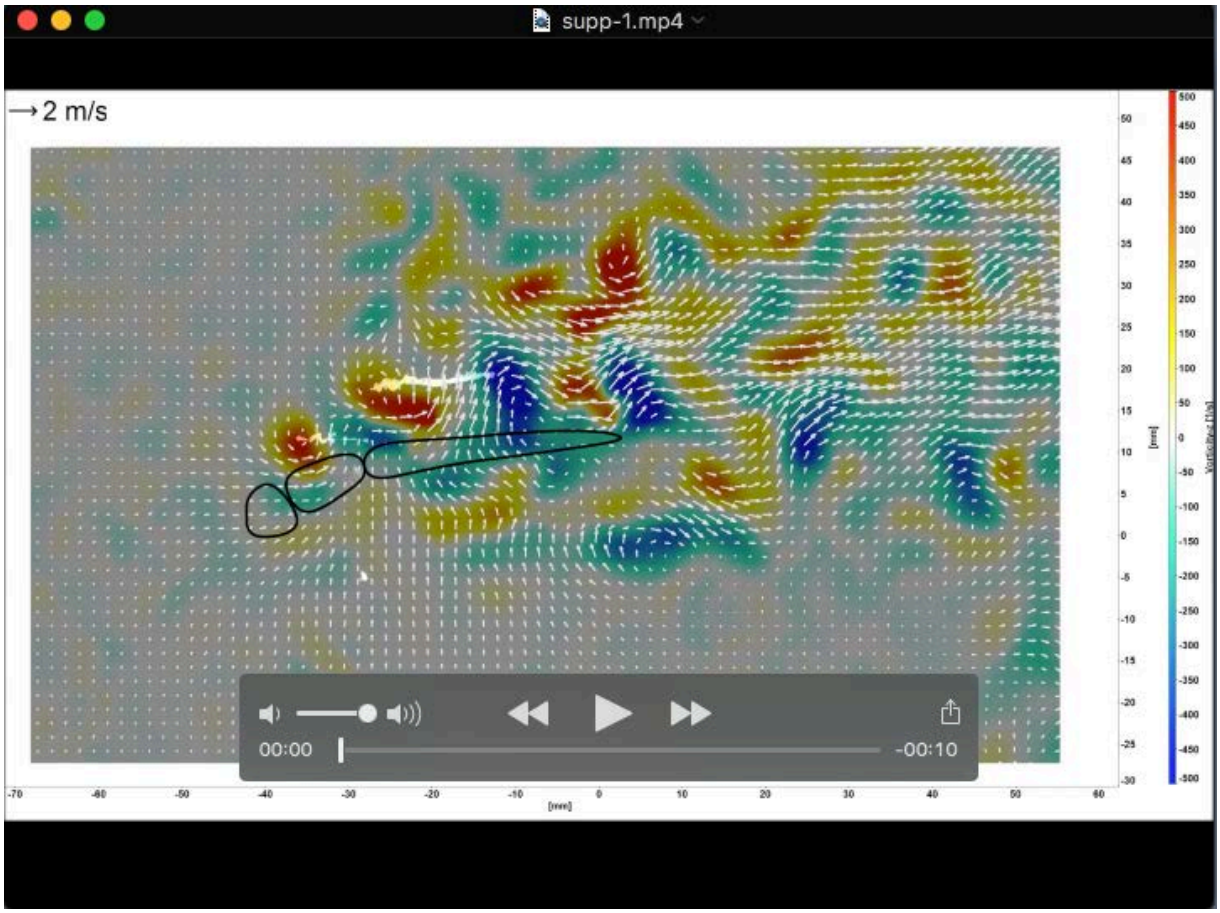

Movie S1. Main flow features of the inner spanwise region (18% S_{HW}) throughout multiple flapping cycles. The synergy between the forewing and hindwing LEVs are observable.

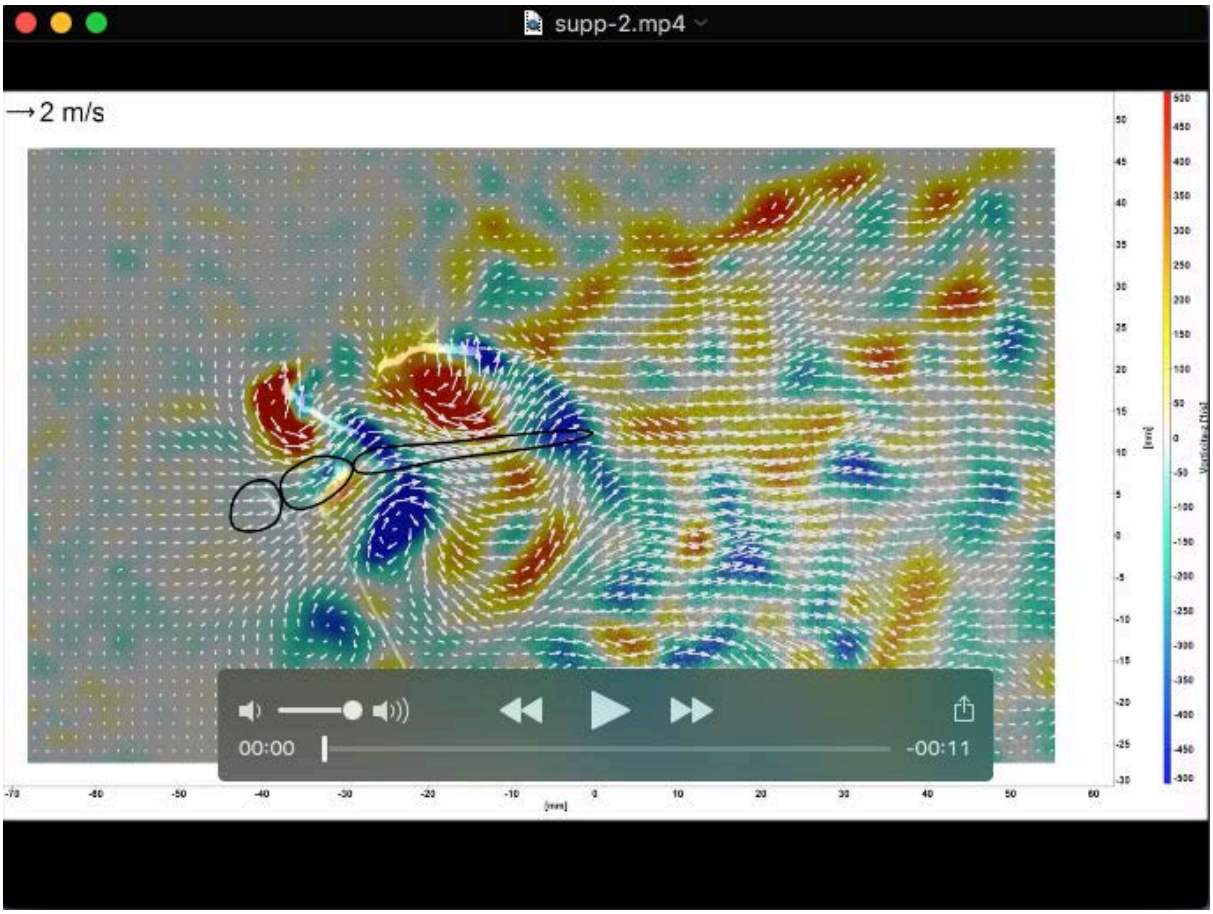

Movie S2. Main flow features in the transition region (42% S_{HW}) throughout multiple flapping cycles. The shed forewing LEV moves downstream below the down-stroking and above the up-stroking hindwing, while having minor effect on the hindwing leading edge aerodynamics. The hindwing LEV formation is delayed, as the hindwing moves through the downwash of the forewing

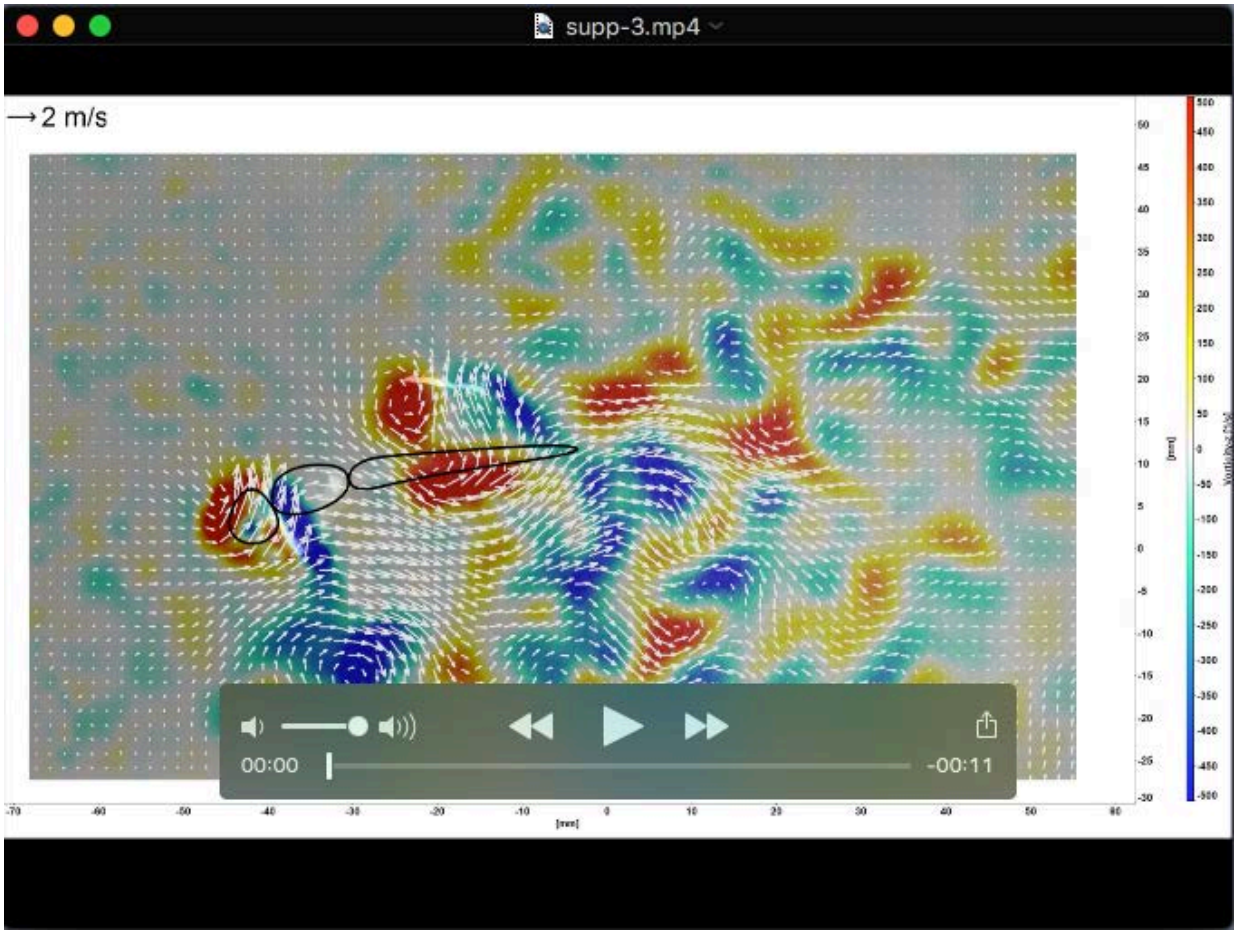

Movie S3. Main flow features in the outer region (78% S_{HW}) throughout multiple flapping cycles.
The LEV formation of the hindwing is suppressed by the downwash of the forewing. The hindwing captures the shed forewing vortex at the end of its stroke. This vortex is anchored to the suction surface of the hindwing and acts as a LEV.